



Graphene-based bimorphs for micron-sized, autonomous origami machines

Marc Z. Miskin^{a,b}, Kyle J. Dorsey^c, Baris Bircan^c, Yimo Han^c, David A. Muller^{a,c}, Paul L. McEuen^{a,b,1} and Itai Cohen^{a,b}

^aKavli Institute at Cornell for Nanoscale Science, Cornell University, Ithaca, NY 14853; ^bLaboratory of Atomic and Solid State Physics, Cornell University, Ithaca, NY 14853; and ^cSchool of Applied and Engineering Physics, Cornell University, Ithaca, NY 14853

Contributed by Paul L. McEuen, November 12, 2017 (sent for review July 20, 2017; reviewed by John C. Crocker and A. John Hart)

Origami-inspired fabrication presents an attractive platform for miniaturizing machines: thinner layers of folding material lead to smaller devices, provided that key functional aspects, such as conductivity, stiffness, and flexibility, are persevered. Here, we show origami fabrication at its ultimate limit by using 2D atomic membranes as a folding material. As a prototype, we bond graphene sheets to nanometer-thick layers of glass to make ultrathin bimorph actuators that bend to micrometer radii of curvature in response to small strain differentials. These strains are two orders of magnitude lower than the fracture threshold for the device, thus maintaining conductivity across the structure. By patterning 2- μm -thick rigid panels on top of bimorphs, we localize bending to the unpatterned regions to produce folds. Although the graphene bimorphs are only nanometers thick, they can lift these panels, the weight equivalent of a 500-nm-thick silicon chip. Using panels and bimorphs, we can scale down existing origami patterns to produce a wide range of machines. These machines change shape in fractions of a second when crossing a tunable pH threshold, showing that they sense their environments, respond, and perform useful functions on time and length scales comparable with microscale biological organisms. With the incorporation of electronic, photonic, and chemical payloads, these basic elements will become a powerful platform for robotics at the micrometer scale.

origami | graphene | bimorph | self-folding | atomic membranes

Self-folding sheets have opened the door to creating complex 3D structures using planar fabrication techniques. Indeed, pioneering experiments have shown how to design self-folding in everything from polymers (1–6) to shape-memory alloys (7). Current state of the art enables self-folding of structures with upward of 100 folds (3), algorithms to map arbitrary 3D structures into 2D fold patterns (8–10), and geometries approaching 100-nm features (7, 11). Beyond static structures, recent work at the centimeter scale has enabled origami robots and mechanisms with broad and useful functions, including locomotion (10) and reprogrammable self-assembly (9).

Here, we extend the conceptual framework of origami fabrication (1–5, 7, 12–17) to the nanoscale: we work with atomically thin sheets, defining the smallest possible size scale for self-folding actuation.

Atomically thin sheets of inorganic, hard materials are ideal for deployable small-scale origami machines, because they combine multiple functional properties into a single platform (18–20). Hard materials are the standard in semiconductor fabrication, and thus, building our actuators around them offers a straightforward route to process integration with other nanotechnologies. Hard materials offer a range of electronic, optical, and chemical functionalities that are well-characterized and tunable. Finally, hard materials possess extreme thermal, chemical, and mechanical stability, assuring that the final devices will be robust to large temperature variations and caustic environments, resist unintended stretching deformations, and bend without creep or stress relaxation. Indeed, the actuators shown here

operate in temperature ranges upward of 140 K and chemical environments spanning at least 13 orders of magnitude in acid concentration.

Our material platform, atomically thin hard material, brings opportunities to reduce origami structures by a factor of 10 without sacrificing key functional properties. Specifically, our actuators are capable of elastically deforming to micrometer-scale folds, producing large force outputs, and electrically linking elements across folds. Looking forward, the capacity to create a network of electrically interconnected actuators that produce sufficient force to support embedded electronics presents opportunities to move away from static origami structures and toward origami robotics at the micrometer scale.

Results

As our prototype design, we engineer graphene and a 2-nm-thick layer of silicon dioxide to function as a bending actuator (Fig. 1). Within the class of hard materials, graphene stands out as an excellent choice, because it is extremely stiff and conductive but also, thin enough to bend to nanometer radii of curvature without fracture (21, 22). Silicon dioxide has an elastic modulus comparable with graphene (80 and 1,000 GPa, respectively) and can be readily fabricated down to nanometer-thick layers. In fact, designing a bimorph for maximum force output, subject to the constraint of elastic response, identifies graphene and a hard, inorganic material, like silicon dioxide, as an optimal combination (*SI Materials and Methods*). Altogether, the stack's total thickness of 2 nm (Fig. 1B) means that it can bend down to ~ 100 -nm radii of curvature before the glass fractures (23) and the device fails. Put differently, strains of only 10^{-4} are needed

Significance

We build origami machines the size of cells by folding them out of atomically thin paper. At the heart of our approach is an actuator technology made from graphene and a nanometer-thick layer of glass. We use these actuators to fold 2D patterns into targeted 3D structures. The resulting machines are freely deployed in solutions, can change shape in fractions of a second, carry loads large enough to support embedded electronics, and can be fabricated en masse. This work opens the door to a generation of small machines for sensing, robotics, energy harvesting, and interacting with biological systems on the cellular level.

Author contributions: M.Z.M., P.L.M., and I.C. designed research; M.Z.M., K.J.D., B.B., and I.C. performed research; Y.H. and D.A.M. contributed new reagents/analytic tools; M.Z.M., K.J.D., B.B., P.L.M., and I.C. analyzed data; and M.Z.M., P.L.M., and I.C. wrote the paper.

Reviewers: J.C.C., University of Pennsylvania; and A.J.H., Massachusetts Institute of Technology.

The authors declare no conflict of interest.

Published under the PNAS license.

¹To whom correspondence should be addressed. Email: plm23@cornell.edu.

This article contains supporting information online at www.pnas.org/lookup/suppl/doi:10.1073/pnas.1712889115/-DCSupplemental.

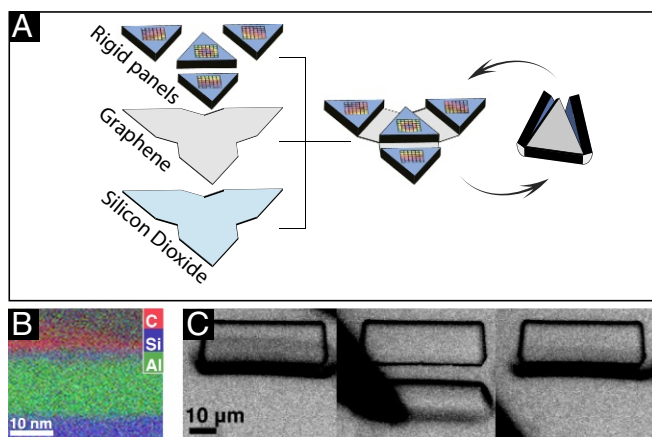


Fig. 1. The basic structure of graphene-glass bimorphs is a sheet of graphene bound to a 2-nm-thick layer of glass (A). The bimorph bends when the glass is strained relative to the graphene. To restrict actuation to take place in specific regions, we pattern in thick pads of photoresist that prevent bending beneath them. The device can then fold and unfold in response to environmental changes. A key parameter in bimorph design is layer thickness: each layer must be of comparable rigidity for the device to bend efficiently. Our glass layers are fabricated to 2-nm thicknesses using atomic-layer deposition. EELS (B) reveals that the glass meets this target size (details are in *Materials and Methods*). During fabrication, the device is attached to the substrate by an aluminum release layer and consequently does not bend. When the release layer is etched away, the bimorphs fold to a specific angle set by the length of the bimorph between the two pads (C). After release, bimorph hinges behave elastically and will spring back to their rest position if loaded and released (*Movies S1* and *S2*). (Magnification: 20 \times .)

to bend to 10 μm , two orders of magnitude below the fracture threshold for the bimorph.

To localize bending to take place in specific regions, thereby producing folds, we pattern, in specific places, rigid 2- μm -thick panels of photoresist (Fig. 1 A and C). These panels remain flat, because they are sufficiently rigid to restrict stretching and bending of the underlying bimorph. By pushing against bent hinges with a probe tip, we find that bimorph hinges are elastic and will spring back to their rest position when released (Fig. 1C). Because of the high stiffness of both graphene and glass, the bimorphs can generate torques large enough to lift the panels, despite the fact that the panels are 1,000 times thicker (*SI Materials and Methods*).

Already, this simple joint shows that inorganic materials offer several key functional requirements for complex micrometer-scale machines. Compared by weight, lifting the panel is equivalent to lifting 500 nm of silicon. This capacity illustrates that graphene-glass bimorphs can produce sufficient force to carry a wide range of payloads fabricated using conventional semiconductor techniques, including photonic structures (24), chemical or biological samples, or information processing technologies (25). Moreover, we find that the graphene in the bimorph retains its unstrained electrical conduction properties when bending. We measure the conductivity across a bent graphene bimorph and gate the current passing through the device by applying a bias voltage to the surrounding electrolyte. Both the measured sheet resistance, $\sim 1 \text{ k}\Omega$ per square, and gating response are typical for unstrained graphene devices (26) (Fig. S1). Indeed these results are expected, as the band structure of graphene does not change appreciably until the applied strains reach a few percentages (27, 28). Altogether, these results show that inorganic materials, as typified by graphene-glass bimorphs, provide key functionalities when thin: they provide high force density actuation, maintain electronic functionality, and can be engineered to bend elastically at micrometer scales.

To build complex structures, we must be able to program how and when actuators fold. This goal requires characterizing how a given bimorph bends in response to different environmental stimuli. By design, the graphene-glass bimorph can bend in response to two different strain control mechanisms: temperature and electrolyte concentration.

Heating a bimorph causes the glass to expand relative to the graphene and bend the device. We show a graphene-glass bimorph held by a tungsten probe surrounded by water in Fig. 2A. We use a laser to locally heat the probe to temperatures on the order of 100 $^{\circ}\text{C}$ (*Materials and Methods*). The induced interlayer strain causes the bimorph to curl to radii of curvature in the range of 1–5 μm (Fig. 2B). Converting the measured curvatures into strain (*Materials and Methods*), we find a linear thermal expansion coefficient mismatch best fit by $2 \times 10^{-6}/\text{K}$, which is typical for bimorphs made from hard materials. Within this temperature range, the strain exerted on the bimorph never exceeds the fracture strain for either graphene (21) or glass (23), indicating that, if the surrounding water is not locally superheated, the water will evaporate before the device fails because of thermal strain.

Beyond thermal actuation, bimorphs can rapidly respond to the local electrolyte concentration because of an ion exchange reaction that takes place within the glass (29–31). Dangling silicon-oxygen bonds can associate with either alkali metal or hydronium ions that diffuse in and out of the glass. If the attaching ion is larger than the size of the surrounding voids, a stress develops wherever an ion associates. For instance, potassium and hydronium are large and are known to swell glass. Conversely, smaller ions, like sodium and lithium, produce far less swelling. This mechanism is commonly used to produce chemically toughened glass (29–31).

We show the behavior of a graphene-glass bimorph when the pH of its surrounding environment is raised from 2 to 10 in Fig. 2C. The bimorph starts curled in the acidic environment,

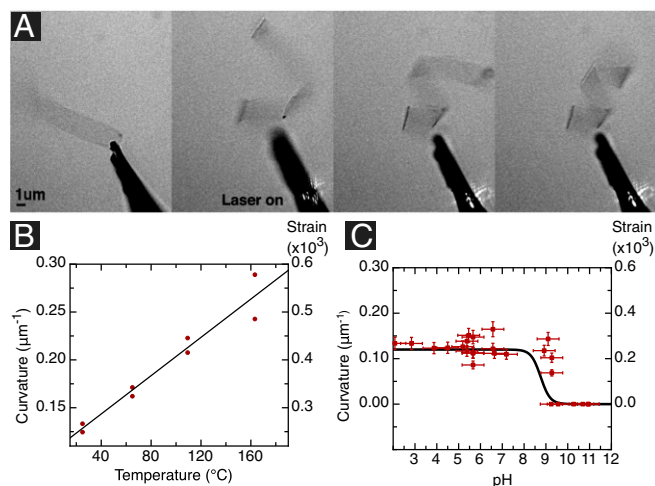


Fig. 2. The strain in a graphene-glass bimorph is a function of both temperature and electrolyte content. (A) A laser heats a probe holding a graphene-glass bimorph. (Magnification: 40 \times .) In response, the glass swells relative to the graphene, and the bimorph coils into a helix with a curvature proportional to the temperature (B). In addition, graphene-glass bimorphs are responsive to pH. In this case, interlayer strain depends on the pH of the surrounding solution and transitions from a finite value to a flat state when a critical pH is exceeded (C). This transition is fully reversible and can be cycled numerous times with the same critical pH setting the unfolding transition. The thermal and chemical mechanisms can be controlled independently and sum together to determine the total strain state in the bimorph. Indeed, the interlayer strain at room temperature in B corresponds to the strain induced by electrolyte effects in C.

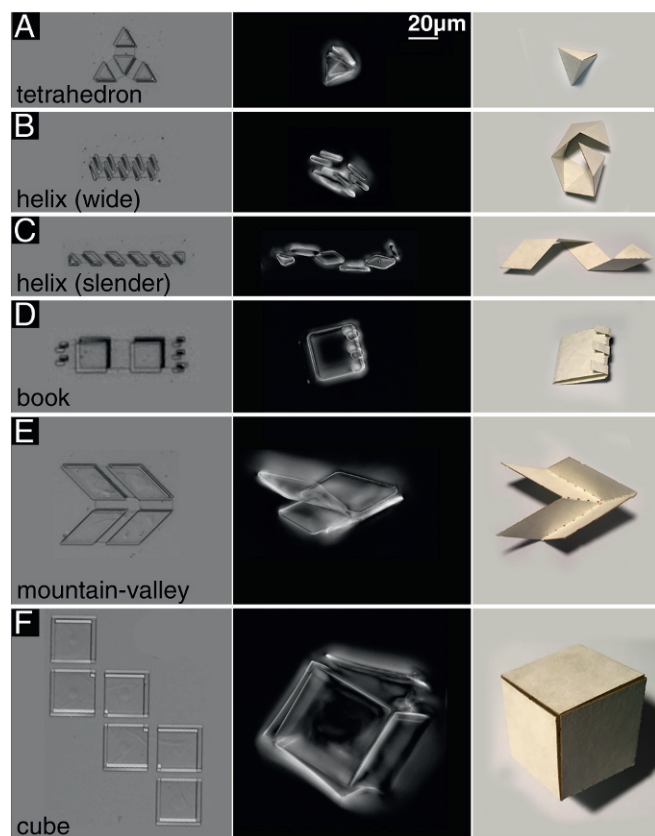


Fig. 3. Graphene-glass bimorphs can be used to fabricate numerous 3D structures at the micrometer scale. These include, but are not limited to, tetrahedron (A), helices of controllable pitch (B and C), high-angle folds and clasps (D), basic origami motifs with bidirectional folding (E), and boxes (F). In *Left*, we show the device flattened and still attached to the release layer. After they are etched, the bimorphs self-assemble to their targeted 3D geometries (*Center*). Images of the folded devices were obtained by focal plane stacking. All of the figures in *Center* are at the same scale. For comparison, we present paper models of the target geometry in *Right*.

but when the pH is raised above pH 9 by adding sodium hydroxide, it unrolls to a flat state. This process is fast (<1 s) and reversible: when the environment is rendered acidic again, the bimorph curls back into a coil. By varying temperature and pH independently, we find that the strain state in the bimorph is a linear combination of thermal stress and chemical stress: devices in basic solutions that start flat fold when heated.

The two ions present in our experiment, sodium and hydronium, exchange with one another within the glass layer of the bimorph to produce the discrete transition in strain. The ratio of their concentrations in the glass is fixed by an equilibrium constant: $pK = -\log_{10} \left(\frac{[\text{SiONa}][\text{H}_3\text{O}^+]}{[\text{SiOH}_3\text{O}][\text{Na}^+]} \right)$. Thus, if enough sodium hydroxide is added to solution, the glass will eventually exchange the large hydronium ions for smaller sodium ions. Assuming that the bimorphs are swollen because of hydronium present in the glass, the strain in the bimorph will be given by (*SI Materials and Methods*)

$$\epsilon = \frac{\epsilon_m}{1 + 10^{-pK+pH-pNa}},$$

where ϵ_m is the maximum strain that results when every dangling bond associated with a hydronium molecule. We show that this equation best fits the data with $pK = 3.5$ in Fig. 2.

This mechanism allows us to shift the pH transition point arbitrarily by independently adjusting the sodium concentration of

the solution. For example, when the salt concentration is held at 1 M, the critical pH should shift from pH 9 to the equilibrium constant $pK = 3.5$. Indeed, when titrating bimorphs in 1 M sodium chloride by adding small volumes sodium hydroxide, the devices unfold at a new critical pH of 3 ± 1 .

The data in Fig. 2 enable us to rationally design 2D material patterns that self-fold into targeted 3D structures. Given a set of environmental conditions, we map the corresponding radius of curvature to a target fold angle by varying the length of bimorph between the rigid panels. Since every bimorph bends the same way, the angle between two panels at a fold is proportional to length of the bimorph between them divided by the bimorph radius of curvature. By varying the span between hinges, we can program specific fold angles. We present a range of structures designed by this approach to self-assemble at room temperature in acidic environments (Fig. 3). We can make polyhedra, including a 20- μm tetrahedron (Fig. 3A) and 50- μm cubes (Fig. 3F). We are able to build helices with programmable pitches (Fig. 3B and C). We can also fold two faces on top of each other and clasp them shut with five interdigitated latches: three on one face and two on the other (Fig. 3D).

Using mathematical constraints from rigid origami design, we can make structures where folds take on positive or negative curvature. For instance, at a fourfold vertex, at most, three folds can be bent upward: the fourth must bend downward if the pads are sufficiently rigid (Fig. 3E, *Right*). We can program which bimorph bends downward by removing material along the width of one hinge (Fig. 3E, *Left*). In this case, the lowest energy state for the system as a whole is to bend this slender bimorph downward against its preferred folding direction (14). We use this scheme to realize the Muira fold, a foundational fourfold vertex used heavily in origami structures, robotics, and metamaterials at the macroscale (3, 10, 12) (Fig. 3E, *Center*).

All of these structures are capable of fast and reversible folding through the pH actuation mode. We show what happens when a concentrated drop of sodium hydroxide is dripped on top of a folded 20- μm tetrahedron in Fig. 4A. The tetrahedron springs open, returning to the flat state in approximately 100 ms. This high-speed motion is a unique feature of working with thin films: for bimorphs driven using either thermal effects or chemical diffusion, response times scale with the square of the layer thickness. For a given material, moving from micrometer- to nanometer-thick films speeds up actuation 1 million-fold. When a drop of acid is added to neutralize the base, the box refolds (Fig. 4B). The process can be repeated multiple times (*Movies S1 and S2*).

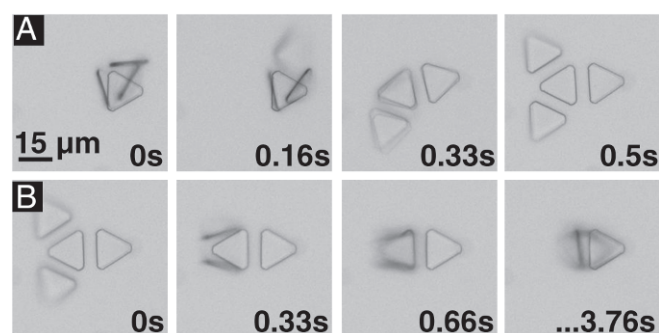


Fig. 4. Devices made from graphene-glass bimorphs can fold and unfold in fractions of a second in response to local pH changes. When the local pH surrounding a folded tetrahedron exceeds the critical unfolding threshold, the device springs open and into the flat state within 0.5 s (A). Changing the surrounding environment to acidic can refold the tetrahedron within 4 s (B).

Discussion

The tetrahedron presented in Fig. 4 displays the fundamental characteristics of an autonomous machine: in response to a stimulus, it consumes energy from its local surroundings to perform useful work. In this case, the tetrahedron converts changes in the environmental chemical potential into mechanical energy. Moreover, it achieves this goal autonomously, executing a preprogrammed response to local changes in its chemical environment.

Moving beyond this proof of concept toward more complex cell-sized machines requires overcoming several challenges. At a fabrication level, work must be done to improve the device yield (typically 10–20% here) and to develop specific processing techniques that seamlessly link nanoscale origami to photonic, chemical, and electronic technologies. At the level of origami systems, future work must develop new actuation schemes to achieve bidirectional folding without leveraging origami constraints, mechanisms to produce sequential folds, and scalable approaches to convert origami fold patterns to fabrication instructions that can be used to construct devices in the cleanroom.

If these challenges can be met, then atomically thin origami presents a route toward micrometer-sized robotics systems comparable in size and speed with microorganisms. For example, the tetrahedron in Fig. 4 fits within a 12- μm radius sphere, making it three times larger than a red blood cell and three times smaller than a large neuron. It senses changes in local electrolyte content in 100 ms, comparable with the timescale that cardiac cells will elevate their membrane potential when triggered. The mechanical stiffness of our bimorph device, $\sim 10^{-5}$ N/m, is comparable in magnitude with the shear and bulk stiffness in cells (32), and the large deflections that our devices can achieve should enable graphene bimorph to locally deform cells to strains on the order of 100%. Finally, graphene, glass, and SU8 polymer are all biocompatible materials that pose no intrinsic toxicity toward cells. Altogether, atomic membrane origami can be used to create a unique class of machines that interact with cells without posing intrinsic chemical or mechanical hazards. Developing additional bimorphs around other hard materials can broaden these capabilities. Each combination presents distinct functionalities and sensitivities, while the chemical, thermal, and mechanical stabilities of the resulting devices greatly exceed the tolerances needed to interface with organic biological systems.

As a platform for microelectronics, the devices depicted in Fig. 3 could carry the key components for computation, sensing, and communication. For example, with 50-nm feature lithography, a full version of the Intel 4004 microprocessor could be assembled to fit within one face of the tetrahedron in Fig. 3A (33). Extrapolating from current commercial memory storage, ~ 30 Mbits of memory could fit on another of the tetrahedron's panels. A fully functional radio frequency identification chip with 128 bits of addressable memory could fit on one panel of the cube depicted in Fig. 3F (34). Moreover, all of these technologies could be integrated with our current fabrication protocol by leveraging advances in chip-bonding and flexible electronics. Ultimately, the size and speed of these devices when combined with the capacity for information processing would present an incredible platform to measure and manipulate matter with precise control on the cellular scale.

Materials and Methods

Bimorph Fabrication. We deposit a release layer onto a clean 170- μm -thick fused silica coverslip. The layers are made from either thermally evaporated aluminum (50- to 250-nm thick) or atomic layer-deposited aluminum oxide (10-nm thick). Next, we use plasma-enhanced atomic-layer deposition at 200 °C to grow 2-nm-thick layers of silicon dioxide. We transfer graphene on top of this stack by wet transferring graphene grown on copper foils. All of the devices are fabricated using polycrystalline graphene grown by chemical vapor deposition (ACS Material), with typical grain sizes ranging from 1 to 5 μm . We spin 4% poly(methyl methacrylate) (PMMA) on top of the

graphene-copper foil, etch the copper with ferric chloride (Transene CE200), rinse the graphene through four baths of deionized water, and transfer it on top of the silica-coated substrates. We then remove the PMMA with an overnight soak in acetone. We pattern devices with photolithography techniques and remove unwanted material with plasma etching. Oxygen plasma is used to etch graphene, while carbon tetrafluoride (CF₄) plasma is used to etch glass. Finally, we release devices by etching away the aluminum in a solution of 10:1 deionized water:HCl. Fig. S4 shows a schematic of our fabrication instructions.

Panel Fabrication. We create panels by spinning SU8 2002 photoresist and soft baking for 1 min at 65 °C followed by 1 min at 95 °C. We expose the resist through a 365-nm filter to a total dosage of 180 mJ/cm² at a wavelength of 356 nm. Next, we hard bake the resist for 1 min at 65 °C followed by 2 min at 95 °C. We develop in SU8 Developer for 1 min, rinse in isopropyl alcohol, and then, rinse in water. Finally, we anneal the panels by ramping devices on a hot plate from 95 °C to 150 °C, holding for 5 min, and cooling the hot plate to ambient.

Characterization of Graphene Grain Structure. The graphene used in the fabrication of our devices was characterized using dark-field EM. Graphene was wet-transferred to 10-nm silicon nitride membranes with 100- μm square windows. Centered dark-field imaging was performed in an FEI Spirit transmission electron microscope (TEM) at 80 keV. A small aperture was placed in the center of the diffraction plane of the microscope, and each diffraction spot was steered through the aperture. Images included in *SI Materials and Methods* are taken from each set of diffraction spots and combined into a composite image. Acquisition times are on the order of 20 s. Domain sizes obtained from these measurements are on the order of a few micrometers.

Characterization of Silicon Dioxide Film Thickness. Samples for cross-sectional scanning transmission EM (STEM) and electron energy loss spectroscopy (EELS) were prepared using focused ion beam (FIB) milling in an FEI Strata dual-beam FIB. To protect samples during this procedure, they were fabricated identically to graphene-glass bimorphs but with the addition of a metal cap (Ti; 50 nm) evaporated on top of the layers under study. Thin lamina were milled from the substrate and attached to a micromanipulator probe. The probe was then brought near a TEM grid, and the lamina was transferred from the probe to the grid. The sample was further thinned with a low-energy ion beam at grazing incidence. STEM and EELS were performed in an FEI Titan Themis STEM at 120 keV. The beam convergence angle was 30 mrad, with a probe current of ~ 15 pA. The EELS spectrum and images were acquired with an energy dispersion of 0.25 eV per channel using a Gatan Quefina dual-EELS spectrometer. A linear combination of power laws was used to fit and subtract the background. The EELS false color composition map was created by integrating the silicon $L_{2,3}$ edge, the aluminum $L_{2,3}$ edge, and the carbon K edge. All of the EELS analyses were done with open source Cornell Spectrum Imager software. Images are included in *SI Materials and Methods*. As the sample is viewed in cross-section, the apparent layer width of a conformal layer is the true layer width blurred with the projected roughness from the substrate; thus, the imaged layer thickness should be viewed as an upper bound.

Thermal Measurements of Bimorph Strain. In our experiments, we use a 1,064-nm laser to locally heat the water around a bimorph. This allows us to superheat the water and achieve temperatures above 100 °C. To characterize the bimorph response, we first measured the curvature of a bimorph as a function of the incident laser power. Next, we heated bimorphs using a temperature-controlled microscope stage to 65 °C. We assume that the change in temperature caused by laser heating is proportional to incident laser power, and by identifying the power setting that leads to the same change in curvature as in the global heating experiments, we are able to produce a conversion factor between incident power and temperature.

Electrical Characterization of Graphene SiO₂ Bimorphs. To measure their electrical properties, we pattern bimorphs into partially released u-shaped geometries (images are in *SI Materials and Methods*). We place two probes onto the device, such that current must pass through the bent portion of the device to complete a circuit. Electrical contact to the devices was made with parylene-coated tungsten microprobes to minimize leakage current through the electrolyte. A dc source-drain bias of 100 mV was applied to the sample with a Yokogawa 7651 voltage source, and the drain current was collected with an Ithaco 1211 current preamplifier. The solution was gated with a silver/silver-chloride electrode.

ACKNOWLEDGMENTS. We thank Mark Bowick, William Dichtel, David Gracias, David Nelson, and Jiwoong Park for insightful discussions. We thank Peter Rose for preliminary experimental work. This work was supported by Cornell Center for Materials Research Grant DMR-1719875, National Science Foundation (NSF) Major Research Instrumentation Award DMR-1429155, NSF

Grant DMR-1435829, Air Force Office of Scientific Research (AFSOR) multidisciplinary research program of the university research initiative Grant FA2386-13-1-4118, and the Kavli Institute at Cornell for Nanoscale Science, and it was performed at Cornell NanoScale Facility, a member of the National Nanotechnology Infrastructure Network (NSF Grant ECCS-0335765).

1. In HJ, Lee H, Nichol AJ, Kim S-G, Barbastathis G (2008) Carbon nanotube-based magnetic actuation of origami membranes. *J Vac Sci Technol B Microelectron* 26:2509–2512.
2. Zhang Q, et al. (2017) Origami and Kirigami inspired self-folding for programming three-dimensional shape shifting of polymer sheets with light. *Extreme Mech Lett* 11:111–120.
3. Na JH, et al. (2015) Programming reversibly self-folding origami with micropatterned photo-crosslinkable polymer trilayers. *Adv Mater* 27:79–85.
4. Yang SY, Choi H-rj, Deterre M, Barbastathis G (2010) Nanostructured origami™ folding of patternable resist for 3D lithography. *Proceedings of the Optical MEMS and Nanophotonics (OPT MEMS) 2010 International Conference*, ed Toshiyoshi H (IEEE, Piscataway, NJ), pp 37–38.
5. Tu H, Jiang H, Yu H, Xu Y (2013) Hybrid silicon-polymer platform for self-locking and self-deploying origami. *Appl Phys Lett* 103:241902.
6. Tibbitts S (2014) 4D printing: Multi-material shape change. *Archit Des* 84:116–121.
7. Rogers J, Huang Y, Schmidt OG, Gracias DH (2016) Origami MEMS and NEMS. *MRS Bull* 41:123–129.
8. Benbernou N, Demaine ED, Demaine ML, Ovadya A (2009) A universal crease pattern for folding orthogonal shapes. arXiv:0909.5388.
9. Hawkes E, et al. (2010) Programmable matter by folding. *Proc Natl Acad Sci USA* 107:12441–12445.
10. Felton S, Tolley M, Demaine E, Rus D, Wood R (2014) A method for building self-folding machines. *Science* 345:644–646.
11. Cho J-H, Gracias DH (2009) Self-assembly of lithographically patterned nanoparticles. *Nano Lett* 9:4049–4052.
12. Silverberg JL, et al. (2014) Using origami design principles to fold reprogrammable mechanical metamaterials. *Science* 345:647–650.
13. Paik JK, Kramer RK, Wood RJ (2011) Stretchable circuits and sensors for robotic origami. *Proceedings of the 2011 IEEE/RSJ International Conference on Intelligent Robots and Systems*, ed Amato NM (IEEE, Piscataway, NJ), pp 414–420.
14. Waitukaitis S, Menaut R, Chen BG-g, van Hecke M (2015) Origami multistability: From single vertices to metasheets. *Phys Rev Lett* 114:055503.
15. Santangelo CD (2017) Extreme Mechanics: Self-folding origami. *Annu Rev Condensed Matter Phys* 8:165–183.
16. Pinson MB, et al. (2017) Self-folding origami at any energy scale. *Nat Commun* 8:15477.
17. Mu J, et al. (2015) Origami-inspired active graphene-based paper for programmable instant self-folding walking devices. *Sci Adv* 1:e1500533.
18. Zhu S-E, et al. (2011) Graphene-based bimorph microactuators. *Nano Lett* 11:977–981.
19. Huang Y, Liang J, Chen Y (2012) The application of graphene based materials for actuators. *J Mater Chem* 22:3671–3679.
20. Conley H, Lavrik NV, Prasai D, Bolotin KI (2011) Graphene bimetallic-like cantilevers: Probing graphene/substrate interactions. *Nano Lett* 11:4748–4752.
21. Lee C, Wei X, Kysar JW, Hone J (2008) Measurement of the elastic properties and intrinsic strength of monolayer graphene. *Science* 321:385–388.
22. Booth TJ, et al. (2008) Macroscopic graphene membranes and their extraordinary stiffness. *Nano Lett* 8:2442–2446.
23. Sharpe W Jr, et al. (2007) Strain measurements of silicon dioxide microspecimens by digital imaging processing. *Exp Mech* 47:649–658.
24. Joung D, et al. (2017) Self-assembled three-dimensional graphene-based polyhedrons inducing Volumetric light confinement. *Nano Lett* 17:1987–1994.
25. Rogers JA, Someya T, Huang Y (2010) Materials and mechanics for stretchable electronics. *Science* 327:1603–1607.
26. Chen D, Tang L, Li J (2010) Graphene-based materials in electrochemistry. *Chem Soc Rev* 39:3157–3180.
27. Pereira VM, Neto AC (2009) Strain engineering of graphene's electronic structure. *Phys Rev Lett* 103:046801.
28. Levy N, et al. (2010) Strain-induced pseudo-magnetic fields greater than 300 tesla in graphene nanobubbles. *Science* 329:544–547.
29. Bradley LC, et al. (2013) Hydronium ions in soda-lime silicate glass surfaces. *J Am Ceram Soc* 96:458–463.
30. Fett T, Guin J, Wiederhorn S (2005) Stresses in ion-exchange layers of soda-lime-silicate glass. *Fatigue Fracture Eng Mater Structures* 28:507–514.
31. Kistler S (1962) Stresses in glass produced by nonuniform exchange of monovalent ions. *J Am Ceram Soc* 45:59–68.
32. Guck J, et al. (2001) The optical stretcher: A novel laser tool to micromanipulate cells. *Biophysical J* 81:767–784.
33. Faggin F, Hoff ME, Mazor S, Shima M (1996) The History of the 4004. *IEEE Micro* 16:10–20.
34. Usami M, et al. (2007) A 0.05 × 0.05 mm² RFID chip with easily scaled-down ID-memory. *Proceedings of the Solid-State Circuits Conference*, ed Fujino LC (IEEE, Lisbon Falls, ME), pp 482–483.